

Continuum bound states as surface states

D. W. L. Sprung, P. Jagiello, J. D. Sigetich

*Department of Physics and Astronomy, McMaster University
Hamilton, Ontario L8S 4M1 Canada*

and J. Martorell

*Dept. d'Estructura i Constituents de la Materia, Facultat Física,
University of Barcelona, Barcelona 08028, Spain*

(November 13, 2018)

We discuss the relation between continuum bound states (CBS) localized on a defect, and surface states of a finite periodic system. We use the transfer matrix method to model an experiment of Capasso, and find all continuum bound and anti-bound states. We compute the rate for intra-subband transitions from the ground state to the CBS and derive a sum rule. Finally we show how to improve the confinement of a CBS while keeping the energy fixed.

I. INTRODUCTION

In 1992, an experiment of F. Capasso et al. demonstrated¹ the existence of well localized continuum bound states (CBS) in a semiconductor superlattice consisting of one thick quantum well surrounded on both sides by several GaInAs-AlInAs well/barrier layers constructed to act as $\lambda/4$ Bragg reflectors. As suggested by Lenz and Salzman², the central well was made double the width of the lattice wells, to act as a $\lambda/2$ Fabry-Perot resonator. Subsequently, Weber³ studied the existence of such states using the transfer matrix method. Among other things, he showed that the Bragg condition need not be very well satisfied for a confined state to exist. B. Sung et al.⁴ have also studied above threshold confined states, in a different material system GaAs/AlGaAs. Radovanović et al.⁵ have written several papers describing mainly numerical methods for tailoring a heterostructure to produce CBS with equal energy spacing, to facilitate second harmonic generation. Finally, Xue-Hua Wang, et al.⁶ have discussed the parity sequence of sub-threshold bound states localized on a defect, and the transition rates between them, but neglecting the variable effective mass.

In this paper we provide further insight into the phenomenon of CBS by relating them to surface states, whose existence was elucidated by Shockley in a deservedly famous paper⁷. An infinite periodic system, illustrated by line (c) of Fig. 1, allows Bloch states with the periodicity of the lattice. If the system is truncated on one side, or on both sides, (line (b)) then one can discuss scattering states with energies above threshold, and bound states below threshold. The transfer matrix method is well adapted to discuss such a periodic system. For convenience we will use the notation of our previous papers^{8,9}.

Among the bound states of a finite periodic array are the Bloch states whose amplitude is spread more or less uniformly over the lattice, and the surface states whose density is confined to the ends. The former usually oc-

cur in the allowed energy bands of the infinite lattice, while the surface states necessarily occur in the forbidden bands. Their wavefunctions decay exponentially outside the array and like $\pm e^{-\theta}$ from cell to cell inside, where θ is the imaginary part of the Bloch phase.

Another way to truncate an infinite lattice is to cut it in the middle and pull the two halves apart. This introduces a defect (line (d) of Fig. 1) which may be either a well or a barrier. As emphasized by Weber³, the condition for a state localized in the central gap of an infinite lattice is that the boundary condition at the edge of the defect matches to a decaying Bloch eigenstate of the unit cell: that is, the wave function will decay by $\pm e^{-\theta}$ from cell to cell. There are also anti-bound states, where the match is to the growing eigenstate. In either case, the Bloch phase must be complex, so such states exist only in the forbidden Bloch zones (FZ).

In section 2, we set up the (generalised) transfer matrix for a system with position-dependent effective mass. In section 3 we apply it to the Capasso experiment. We determine the width of the central well/barrier to provide a CBS at a desired energy. In sec. 4 we discuss the relation between these states and states in a box, illustrated in frames (a) and (f) of Fig. 1. In Sec. 5 we show how to compute the transition rate from the ground state to continuum states in the neighbourhood of the CBS, and derive a sum rule which implies that the total strength depends very little on the number of cells involved. Finally, in Sec. 6 we propose new experimental configurations that improve the confinement of a CBS while keeping the energy fixed.

II. TRANSFER MATRIX

Consider solutions of the Schrödinger equation with a variable effective mass

$$-\frac{\hbar^2}{2} \frac{d}{dx} \left(\frac{1}{m(x)} \frac{d}{dx} \psi \right) + (V(x) - E)\psi = 0 \quad (1)$$

At a discontinuity of the potential or of the effective mass, both $\psi(x)$ and $\psi'(x)/m(x)$ are continuous. Let $v(x)$ and $w(x)$ be any two independent solutions at the same E . Then the modified Wronskian

$$w(x)\frac{v'}{m(x)} - v(x)\frac{w'}{m(x)} = C \quad (2)$$

takes a constant value. We choose $C = 1$ by suitable normalization.

For convenience we will discuss the situation where the entire system has reflection symmetry. Then it is sufficient to consider solutions only for $x > 0$ and reflect them in the origin. In many cases, including the specific examples discussed by Weber, Capasso and Wang et al., it is possible also to choose the unit cell to have reflection symmetry about its midpoint. We will do this when it aids in the analysis.

We factorise $m(x) = m_e m^*(x)$ into the bare mass m_e and the dimensionless m^* . The constant $\hbar^2/2m = 3.81$ eV \AA^2 converts from energy to length units. In Weber's model both the potential and the effective mass are piecewise constant functions, but the method is valid even if $V(x)$ and $m^*(x)$ vary continuously within the cell.

Consider a solution $v(x)$ which has value 1, slope 0 at the left edge of the unit cell, and another solution $w(x)$ which has value 0 and slope $m^*(0)$ there. The transfer matrix for the unit cell of the lattice is then

$$W(0 \rightarrow d) = \begin{pmatrix} v & w \\ v'/m^* & w'/m^* \end{pmatrix} \quad \text{with} \\ \begin{pmatrix} \psi \\ \psi'/m^* \end{pmatrix}_d = W(0 \rightarrow d) \begin{pmatrix} \psi \\ \psi'/m^* \end{pmatrix}_0. \quad (3)$$

Here the solutions v, w without argument are evaluated at the cell edge, $x = d - 0$, and ψ is an arbitrary solution. In a periodic system, $W(d)$ depends only on the length of the cell, not its position. Since ψ and ψ'/m^* are continuous at interfaces, to move one interval further to the right one simply multiplies again by the appropriate transfer matrix. Any discontinuity in the derivative is automatically taken into account.

Eigenvalues of the transfer matrix satisfy

$$\lambda^2 - 2 \cos \phi \lambda + 1 = 0 \quad \text{where} \\ 2 \cos \phi \equiv \text{Tr } W = v + w'/m^*, \quad (4)$$

and when the Bloch phase ϕ is a real angle, they are $\lambda = e^{\pm i\phi}$. Generally, raising the energy from the potential minimum, one is in a forbidden band where $|\cos \phi| > 1$. In this region of energy, $\phi = i\theta$ is imaginary. Following this, the first allowed band occurs within which ϕ increases from zero to π . Then in the next forbidden band, with $\cos \phi < -1$, $\phi = \pi + i\theta$ becomes complex. In the p 'th forbidden band, $\phi = p\pi + i\theta$ and the eigenvalues are $\lambda = (-)^p e^{\pm \theta}$.

A. Surface States

Because we have assumed that parity is a good quantum number, states of the whole system will have either even or odd parity. Suppose that the infinite array is truncated so that there are N cells to right of the origin as in Fig. 1, frame (b). Then the condition for a bound state is that the wave function at the right edge of the array matches to a decaying solution outside. (Here we suppose constant potential outside, but that can be changed trivially.)

$$\begin{pmatrix} \psi \\ \psi'/m^*(d) \end{pmatrix} \Big|_{Nd} = W^N \begin{pmatrix} \psi \\ \psi'/m^*(0) \end{pmatrix} \Big|_0 \quad (5)$$

For an even bound state, $\psi = v(x)$, on the right hand side W^N acts on $(1, 0)$ while for an odd state $w(x)$ it acts on $(0, 1)$. This gives the log-derivative

$$\frac{\psi'}{m^*(d)\psi} \Big|_{Nd} = \frac{W_{2s}^{(N)}}{W_{1s}^{(N)}} = \frac{-\kappa}{m_{out}^*} \quad (6)$$

where $s = 1 (2)$ for even (odd) states, and $m^*(d)$ is the effective mass inside the edge of the last cell, while m_{out}^* is the value outside, and $E = V_{out} - \hbar^2 \kappa^2 / (2m m_{out}^*)$. By construction, the W -matrix is real, so the energy E must lie below the external potential V_{out} . On the other hand, a surface state can exist only when E is in a forbidden zone, with complex $\phi = p\pi + i\theta$. In such a zone⁸,

$$W(Nd) = W^N(d) \\ = (-)^{(N-1)p} \left[\frac{\sinh N\theta}{\sinh \theta} W - (-)^p \frac{\sinh(N-1)\theta}{\sinh \theta} \right] \quad (7)$$

Eqs. 6, 7 allow one to search for energies where surface states occur.

B. Continuum Bound States

Suppose that the infinite periodic array is cut at the origin and an extra well of width $2c$ is placed between the two sections, as in frame (d) of Fig. 1. Let $T(c)$ be the transfer matrix (as in eq. 3) that takes the wave function from the origin to c . Its columns are the even and odd parity solutions within the central well. In order for a CBS to exist, the first (or second) column of $T(c)$ must match to a decaying eigenstate of the unit cell of the semi-infinite array to the right. In other words, one of the columns of $T(c)$ must satisfy the eigenvalue equations for $W(d)$ ³:

$$(W(d) - \lambda I) \begin{pmatrix} \psi(c) \\ \psi'(c)/m^* \end{pmatrix} = 0 \quad (8)$$

$$\begin{aligned}\frac{\psi'(c)}{m^*(c)\psi(c)} &= \frac{\lambda - W_{11}(d)}{W_{12}(d)} \\ &= \frac{W_{21}(d)}{\lambda - W_{22}(d)}.\end{aligned}\quad (9)$$

Either of these equations can be used to search for CBS. If they are satisfied with real λ being the smaller (larger) eigenvalue, then a CBS (or an anti-bound state, (ABS)) exists at that energy. The only difference between them and surface states is the numerical value of the boundary condition that has to be satisfied where the lattice meets the defect, or the surface.

III. CAPASSO-WEBER EXAMPLE

The array constructed by Capasso can be modelled as a sequence of potential wells of width $a = 16\text{\AA}$, depth $V_w = 0$ and barriers of width $b = 39\text{\AA}$, height $V_b = 500$ meV. The energy-dependent effective mass in each layer is given by¹¹

$$\begin{aligned}m_w^* &= 0.043(1 + (E - V_w)/E_w) \\ m_b^* &= 0.073(1 + (E - V_b)/E_b)\end{aligned}\quad (10)$$

where $E_w = 0.88$ eV, and $E_b = 1.49$ eV are the effective band gaps of the InGaAs wells and AlInAs barrier materials.

In this example, the potential is piece-wise constant, so the transfer matrix can be constructed from factors of the type

$$T(c) = \begin{pmatrix} \cos kc & m_c^* \sin kc/k \\ -k \sin kc/m_c^* & \cos kc \end{pmatrix}\quad (11)$$

where $k^2 = 2m_e m_c^*(E - V_c)/\hbar^2$ is the wave number inside the layer and m_c^* is the effective mass there. In contrast to Weber, we find it convenient to define the unit cell as a half-well of width $a/2$ on each side of a barrier of width b : then

$$W(d) = T(a/2)T(b)T(a/2)\quad (12)$$

is the transfer matrix of a symmetric unit cell, and has both diagonal elements equal to $\cos \phi$. Panel (a) of Fig. 2 shows a part of the array.

In Fig. 3, we show the eigenvalues in the forbidden zones. To guide the eye, they are connected by straight lines across the allowed zones. There is an even index forbidden zone up to 307 meV in which the eigenvalues vary enormously. The odd FZ from 387 to 641 meV shows a smaller but still appreciable range of variation. This is reduced still further in the third FZ from 881 to 960 meV. The smallest values of $|e^{-\theta}|$ occur near the middle of the forbidden zones.

The transfer matrix from the origin to $c + Nd$ is $W^N(d)T(c)$. For any non-zero c the central well constitutes a defect in the superlattice. If $N \rightarrow \infty$, the

argument of Sec. 2B applies, and the wave function will only be localized near the origin when one of the columns of $T(c)$ is an eigenvector of $W(d)$ with the decaying eigenvalue $\pm e^{-\theta}$. The left hand side of eq. 9 (cf. eq. 11) is either $-k_w \tan k_w c/m_w^*$ (for an even state), or $k_w \cot k_w c/m_w^*$ (odd state). But the identity $\cot(x + \pi/2) = -\tan(x)$ means that the solutions for odd states can be found simply by adding $\pi/2$ to the value of $k_w c$ of an even state solution. Given any solution, another one which differs only by the number of nodes in the central well, can be obtained by adding π/k_w to c . Hence, it is the *differences* in width of the central well that go by half-wavelengths, not the whole width.

By solving

$$\begin{aligned}\tan k_w c &= \frac{W_{11}(d) - \lambda m_w}{W_{12}(d) k_w} \\ &= \frac{W_{21}(d) m_w}{W_{22}(d) - \lambda k_w}\end{aligned}\quad (13)$$

we obtain the values of c in Fig. 4 where we plot the solutions from the principal branch of the arctan function. In the first (even) FZ, lines 2 and 4 reach the $c = 0$ axis at the beginning of the allowed zone, at 641 meV. In our convention, $c = 0$ makes the central well have total width $a = 16\text{\AA}$, the same as in the infinite SL, so one has a periodic system in which no confined state exists. That is why the loci of CBS or ABS terminate on the line $c = 0$ at either end of a forbidden zone.

The horizontal dotted line at $c = 8\text{\AA}$ picks out the odd CBS state at 563 meV found by Weber and Capasso. In this case, the central well is double the width of the wells in the lattice. Very close by at 577 meV is an even ABS (line 3). In the next odd-parity FZ there is an odd parity CBS at about 890 meV.

Fig. 5 allows one to read off the energies of the CBS (ABS) for any choice of width c . Line 2 is just line 1 augmented by $\pi/(2k_w)$; similarly for lines 4 and 3. Negative values of c down to $-a/2$ are meaningful, as they simply shrink the width of the central well down to zero. The straight line segments across the allowed zones are drawn just to connect related solutions.

Because the choice of a flat central potential leads to the tangent function in eq. 13, one can invert to obtain c directly. For a more complex potential one would have to search for solutions of eq. 9, but nothing would change in principle. Any potential that produces the same boundary condition at c gives the same solution, with only the details of the wave function between $\pm c$ changing. For example, Wang et al.⁶ used a two-segment well/barrier combination as their central well. Its boundary value still varies between $\pm\infty$, so one must expect similar solutions, albeit at slightly different energies.

As explained by Shockley⁷, (see also⁹) a unit cell which is more attractive at the edges than in the centre, is just the type which favours the occurrence of surface states. Compared to a well of constant average depth, the energies of even states are raised and those of odd states, low-

ered. This leads to band mixing in the forbidden zones, making it possible for the decaying eigenstate of the cell to match to a decaying exponential with a positive log derivative of ψ at the outer edges. In the Capasso device, it is the odd state in the central well which has the positive log derivative where it matches to the lattice on the right, making the CBS. Viewed from the lattice, at the left edge the match is to a fast decreasing wave function in the central well, which must vanish at the origin.

To illustrate the close relationship between CBS and surface states, in Fig. 6 we show in the upper panel the right side of a six cell lattice with the central well of width $2a$, having the CBS at 563 meV. In the lower part we show a three cell lattice with a surface state at the left edge decaying into the potential barrier, chosen so the slope is exactly the same for both wave functions. The only difference is that one state goes to zero at the origin to make an odd parity wave function, while the other decays exponentially; within the lattice they are identical.

As a second example, we replaced the central well by a central barrier, (see Fig. 2b) similar to the system proposed by Lenz and Salzman². In this case the unit cell is taken to be a barrier of width $b/2$ on either side of a well of width a . The diagonal elements of $W(d)$ are interchanged but its trace is unchanged, so the band structure is identical. In Fig. 7 we show the corresponding results for the extra barrier-width c . As before, $c = 0$ corresponds to a periodic system and no CBS is possible, as this point comes at the edge of an allowed band. The central barrier pushes up the energies of even parity states, so now an even-parity CBS is found in the neighbourhood of 550 meV, with $c \sim 20\text{\AA}$. There is a nearby odd-parity ABS if $c > 17\text{\AA}$.

To see whether the thicknesses chosen by Capasso were optimal, we varied b and a . For fixed well width a , the area enclosed by the eigenvalues of the odd FZ in Fig. 3 expands continually as b is increased, even to 200\AA . The lowest absolute value of the smaller eigenvalue $|\lambda_-|$ gets smaller and smaller: see Table I. However, this simply means that the wells become progressively decoupled as the distance between them gets larger. Similarly, for fixed barrier width $b = 39\text{\AA}$, $|\lambda_-|$ decreases steadily as the well width increases, while the energy of the CBS moves down towards threshold. At $a = 20\text{\AA}$ it becomes a true bound state below threshold. For $a = 19\text{\AA}$, $|\lambda_-| = 0.2508$ which is almost twice the rate of decay of probability (which depends on $|\lambda|^2$) from cell to cell within the lattice, as compared to $a = 16\text{\AA}$. The energy of the CBS is then at 506 meV. The values $k_w a = 1.810$ and $k_b b = 0.426$ are even further from the Bragg condition than for the original parameter set. This confirms Weber's finding that a high degree of confinement does not require exactly satisfying the Bragg condition.

For a central barrier, the behaviour with increasing barrier width is similar to what was found above for a central well: see Table II. Here it is an even parity CBS that falls in energy from 778 to 503 meV as b increases

from 20 to 100\AA . But again, this is a result of decoupling of the wells. For fixed $b = 39\text{\AA}$, there is a shallow minimum of $|\lambda_-| = 0.351$ at $a = 17\text{\AA}$ and the energy of the CBS is at 574 meV. Again, $k_w a = 1.757$ and $k_b b = 1.505$ are far off the Bragg condition.

However, the conclusion is very different if both a and b are varied while keeping the energy of the CBS fixed. An example is shown in Table III. The minimum value of $|\lambda_-|$ is obtained with both $k_w a$ and $k_b b = \pi/2$. It should be expected because, once we fix the energy of the state, the effective mass is also fixed. Then the optimization of $k_w a$ and $k_w b$ proceeds exactly as for an energy-independent Kronig-Penney potential, for which the Bragg condition is optimal, as one can easily show analytically.

IV. RELATION TO STATES IN A BOX

Kalotas and Lee¹² considered the states obtained by enclosing a finite number of cells between infinite walls. (See frames (a) and (f) of Fig. 1 for an illustration.) This discretizes the continuum, so all states become discrete. Well localized states that decay quickly enough will be scarcely affected by the walls. States spread over the whole lattice will become a discrete set maintaining a similar character. An ABS whose magnitude grows away from the origin will be squeezed against the walls of the box.

In order for the finite N system to agree with Weber's, we add an extra half-well or barrier at the right edge of the array. Fig. 8 shows an example where we have taken $N = 10$ cells on each side of the origin. This is to be compared with the CBS at $E = 563$ meV of the $c = 8\text{\AA}$ example of Capasso and Weber. Even with just three cells on either side, the state is hardly shifted from its position in the infinite array.

In Fig. 9 we show the spectrum of box states as a function of N , again for the $c = 8\text{\AA}$ central well case. The energies of the single-cell states change little as more cells are added. The new states that appear fill up the allowed bands. To understand this, it is convenient to consider a system with a hard wall at the origin, then N identical cells, followed by a hard wall at the right. The allowed wave functions are those that vanish at the origin (odd-parity states of the symmetric system), and the hard-wall boundary condition at the right edge is $\psi(x = Nd) = 0$. In view of eq. 5, this requires that the element $W_{12}(Nd) = 0$. Since in an allowed band

$$W^N(d) = \frac{\sin N\phi}{\sin \phi} W(d) - \frac{\sin(N-1)\phi}{\sin \phi} I, \quad (14)$$

this can be written

$$W_{12}^{(N)} = 0 = \frac{\sin N\phi}{\sin \phi} W_{12}(d) \quad (15)$$

This shows that bound states can occur in either of two ways. First, as single-cell bound states, where the second

factor vanishes. These states have N nodes, and the wave function vanishes at every cell boundary. Alternatively, the combinatorial factor $\sin N\phi/\sin\phi$ might vanish, and in an allowed band there are $N-1$ such states where $N\phi = m\pi$, $m = 1, 2, \dots, N-1$. The single-cell state may occur in a forbidden zone, but the others can only occur for real ϕ , in an allowed band. For non-zero c one has to multiply $W^N(d)$ from the right by the additional transfer matrix $T(c)$ for the central well, and then the simple factorization won't be exact. In practice the states tend to remain in the allowed band all the same.

Fig. 9 provides another example of the similarity of CBS and surface states. In the upper panel (a), the CBS lies in the middle of the first of the first forbidden zone, while in the lower panel there are two such states, one derived from allowed band α and the other from band β .

V. TRANSITION RATES

Introducing the vector potential into the Hamiltonian eq. 1 leads to the excitation operator

$$\frac{eA}{2c} \left[p \frac{1}{m(x)} + \frac{1}{m(x)} p \right] \equiv \frac{-i\hbar eA}{2m_e c} S \quad (16)$$

with dimensions of energy. In defining the operator S , (dimensions inverse length) we have factored out the bare electron mass, leaving only the dimensionless effective mass ($m^* \sim 0.06$) inside. The vector potential A is assumed to be a function of x , so it commutes with the mass. By invoking the Coulomb gauge we make it commute with the momentum as well.

According to the Golden rule, the transition rate is

$$w_{if} = \frac{2\pi}{\hbar} \left(\frac{eA\hbar}{2m_e c} \right)^2 |\langle \Psi_f | S | \Psi_i \rangle|^2 \rho(E_f), \quad (17)$$

where $\rho(E_f)$ is the density of final states. The factors before the matrix element have dimensions length squared energy per second, and these are omitted from our calculations. The matrix element squared times the density of states is therefore (energy length-squared) $^{-1}$, and this is what we plot in Fig. 10 for example. After integrating over energy, we have units \AA^{-2} for the total strength.

In the Capasso experiment, the ground state has even parity, so its derivative is odd, and transitions are allowed only to odd parity excited states. Also the lattice is finite rather than infinite, so the transitions are to states in the continuum. In the neighbourhood of the CBS, the continuum wavefunction has a large normalization inside the central well, and this causes the transition rate to peak at or near this energy.

We again consider the case of a central well of half-width c surrounded by N cells on each side. But for convenience, in this section we follow Weber by defining $W(d) = T(a)T(b)$ as having a barrier of width b on the left followed by a well of width a . Then N will be the

number of wells additional to the central well. The odd parity excited state with Dirac delta-function normalization has wave function

$$\begin{aligned} \Psi_f(x) &= B_0 \sin(k_w x) \quad , \quad |x| < c \\ &= \frac{1}{\sqrt{\pi}} \sin(k_b x + \delta) \quad x > c + Nd. \end{aligned} \quad (18)$$

where $E - V_b = \hbar^2 k_b^2 / (2mm_b^*)$ measures the energy above the top of the barrier in the asymptotic zone, and $k_w^2 = 2mm_w^* E / \hbar^2$ is the wave number inside the central well. Using the transfer matrix $W(d)$ to cross N cells gives

$$\frac{1}{\sqrt{\pi}} \begin{pmatrix} \sin(k_b(c + Nd) + \delta) \\ \nu_b \cos(k_b(c + Nd) + \delta) \end{pmatrix} = B_0 W^{(N)} \begin{pmatrix} \sin k_w c \\ \nu_w \cos k_w c \end{pmatrix}, \quad (19)$$

where $\nu_w = k_w/m_w^*$, $\nu_b = k_b/m_b$ and $W^{(N)} = W^N(d)$, so that:

$$\frac{1}{\nu_b} \tan(k_b(c + Nd) + \delta) = \frac{W_{11}^{(N)} \sin k_w c + W_{12}^{(N)} \nu_w \cos k_w c}{W_{21}^{(N)} \sin k_w c + W_{22}^{(N)} \nu_w \cos k_w c} \quad (20)$$

determines δ and

$$\frac{1}{\sqrt{\pi}} \sin(k_b(c + Nd) + \delta) = B_0 (W_{11}^{(N)} \sin k_w c + W_{12}^{(N)} \nu_w \cos k_w c) \quad (21)$$

gives the normalization B_0 . Note that the matrix elements of $W^{(N)}$ can be easily computed from those of $W(d)$ using eq. 7 (or eq. 14 when the Bloch phase ϕ is real). One need not solve explicitly for the phase shift $\delta(E)$ because only $|B_0|^2$ is required to compute the transition rate, and the identity $\sin^2 z = \tan^2 z / (1 + \tan^2 z)$ can be used in eq. 21.

With the above equations we can construct the wavefunction $\Psi_f(x)$ as follows. Wave functions $v(x)$, $w(x)$ in a unit cell of the lattice are defined in eq. 3. Within the r 'th cell following $x = c$, ($r = 1, 2, \dots$) the wave function $\Psi_f(x)$ is

$$\Psi_r(x) = A_r v(x - c - rd + d) + B_r w(x - c - rd + d) \quad (22)$$

and from the matching at $x = c$ we have: $A_1 = B_0 \sin k_w c$, $B_1 = B_0 \nu_w / \nu_b \cos k_w c$. In general,

$$\begin{pmatrix} A_{r+1} \\ B_{r+1}/m^* \end{pmatrix} = W(d) \begin{pmatrix} A_r \\ B_r/m^* \end{pmatrix}, \quad r = 1, \dots, (N-1). \quad (23)$$

This gives values of $\Psi_f \rightarrow \Psi_r(x)$ in each cell and allows the calculation of the matrix element in eq. 17.

The ground state wave function is computed in a similar manner. Inside the central well it is

$$\Psi_0(x) = N_0 \cos(k_w x) \quad , \quad |x| < c \quad (24)$$

and at $x = c + Nd$ it must match to a decaying exponential, as in eq. 6. If the state is well bound it is a good approximation to use the Kalotas state which vanishes at the edge of the lattice or the Weber state that in principle extends to infinity. The normalization constant N_0 must be computed by summing the normalization integrals from every cell as well as from the central well. If one integrates $\langle v|v \rangle$, $\langle v|w \rangle$, and $\langle w|w \rangle$ over the unit cell, then it is just a matter of multiplying these integrals by the coefficients in the r 'th cell and summing.

Because the effective mass depends both on position and momentum, it is not obvious how to evaluate the matrix elements of the transition operator S . It is reasonable, in the term p/m^* to let the p act on the excited state ψ_E and interpret the effective mass as being at that energy. Conversely, in the $(1/m^*)p$ term, where the p acts on the initial state, we use the ground state effective mass m_0^* . Then,

$$\begin{aligned} \langle \psi_E | S | \psi_0 \rangle &= - \int_a^b \frac{d\psi_E}{dx} \frac{1}{m^*(E)} \psi_0 dx + \\ &\int_a^b \psi_E \frac{1}{m^*(E_0)} \frac{d\psi_0}{dx} dx \end{aligned} \quad (25)$$

Since ψ'/m^* is continuous at interfaces between wells and barriers, the integrand is continuous, despite the jumps in m^* . When the effective mass m^* is piece-wise constant, we can evaluate the integral over a series of intervals of constant m^* (here interpreted as the $m^*(x, E)$).

The squared matrix element, including the density of states factor, is plotted as a function of energy in Fig. 10, which is to be compared with Fig. 2 of Sirtori et al.¹. (However, their figure has normalized the peak intensity to unity in each case, obscuring the fact that the integrated strength is constant.) As the number of side wells increases, the computed excitation function rapidly becomes very narrow. (The experimental width is much larger than theory, indicating that something else is happening.) It shows that even a small number of cells is sufficient to give a well confined state. We also find increasing strength in the second allowed band near 700 meV as cells are added. The integrated strength under the main peak (from 500 to 640 meV) varies only a few percent.

To illustrate how the continuum wave functions evolve in the region of the CBS, we show in Fig. 11 four cases spanning the energy range. It can be seen that as one passes over the CBS energy at 563 meV, an additional node appears in the wave function. Away from this resonance, (panels (a), (b)) the wave function consists mainly of the growing solution in the lattice, so the amplitude is largest at the outside edge (where it is fixed, according to eq. 18). Close to the CBS, (panel (c)), there is

a large component of the decaying solution, making the amplitude in the central well large. Increasing the energy again, (d), brings back more of the growing solution. At 577 meV, the position of the ABS, only the growing solution would contribute. If we had more than $N = 3$ cells, the effects would be even more pronounced.

While the peak in the transition strength becomes very narrow as the number of lattice cells N increases from zero to 3, the integrated strength is almost constant. This can be understood from the sum rule which follows from eq. 17, and is discussed in the appendix. The total strength, M_2 , is defined in eq. A2. In addition to the integral over the continuum, when there are N Bragg reflectors on either side of the central defect, there will be N discrete odd-parity bound states, which must also be included in the sum. Typically these account for something like 6% of the total strength. These odd bound states are shown in Fig. 12, for the case $N = 2$. In this figure, the wave functions are remarkably similar inside the region where the ground state is large, so they give almost equal contributions to the sum rule.

Turning now to the results, one has to distinguish between the no-reflector case and the N -reflector case. In the former, the integrated transition strength (ITS), M_2 , is about 1.4\AA^{-2} . The strength is very broadly distributed above threshold; see line (a) in Fig. 10. We have looked at $N = 1$ to 5 cells on each side. For these cases, the ITS is around 1.35\AA^{-2} , of which about 0.09 comes from the bound odd-parity excited states. As N increases, the ITS fluctuates only a little. The strength remains highly concentrated into the CBS peak (about 80%), the remainder being spread quite widely (6% in the bound states and 14% in the continuum).

Because the CBS peak becomes so narrow, we estimate the integral under it by assuming a Breit-Wigner shape, and deducing the height and width from the calculations.

The sum rule, calculated according to eq. A3, is always about 6 to 10 % higher than the ITS, if we (arbitrarily) set the doorway state mass m_E to be at $E = E_{CBS} = 563$ meV. The main term in eq. A3 is proportional to $(1/m_0 + 1/m_E)^2$, so we can easily adjust the doorway energy to ensure that the sum rule will agree with the ITS. We call this the effective doorway energy E_D . With no reflectors E_D is about 740 meV (535 above the ground state energy). This is reasonable since the excitation strength is very broadly distributed above threshold. With one reflector (on each side), E_D drops to 660 meV; but then it slowly rises, at least up to $N = 5$, where it reaches 670 meV.

VI. OPTIMAL CBS CONFINEMENT

In this section we discuss some general principles for designing a well confined CBS. Consider a general unit cell of width d , within which the potential and the effective mass are arbitrary functions of x . (Since we will fix

the CBS energy, this allows for energy dependence of the effective mass.) Now let us arbitrarily divide the cell into two parts so that the widths a and b add to d , and denote by W^a , W^b the transfer matrices of the two parts. When a is on the left, we have $W^d = W^b W^a$, with elements

$$W_{ij}^d = W_{i1}^b W_{1j}^a + W_{i2}^b W_{2j}^a \quad (26)$$

If the whole array is symmetric about the origin, there will be two type- a portions together at the origin, and the sequence of potentials is $\dots baba\dots ba|ab\dots abab\dots$. When we look for odd parity confined states of such an array, it is equivalent to putting a hard wall at the origin, and solving only the right side. The wave function at the edge of the first cell will be, using eq. 3

$$\left(\begin{array}{c} \psi \\ \psi'/m^* \end{array} \right) \Big|_d = \left(\begin{array}{c} W_{12}^d \\ W_{22}^d \end{array} \right) = \lambda \left(\begin{array}{c} 0 \\ 1 \end{array} \right) \quad (27)$$

The second equality holds if we imagine an infinite array, and demand an eigenstate with the wave function in each cell differing only by a factor λ . This wave function will vanish at both $x = 0$ and d , and in the second cell, the value of ψ'/m^* will differ by a factor λ from the first. The condition that must be satisfied is $W_{12}^d = 0$, and then $\lambda = W_{22}^d$. Writing these out in terms of the component transfer matrices gives

$$\begin{aligned} W_{12}^d &= W_{11}^b W_{12}^a + W_{12}^b W_{22}^a = 0 \quad \text{or} \\ \frac{W_{11}^b}{W_{12}^b} &= -\frac{W_{22}^a}{W_{12}^a} \quad \text{and} \\ W_{22}^d &= W_{21}^b W_{12}^a + W_{22}^b W_{22}^a = \lambda \\ &= \left(W_{21}^b + W_{22}^b \frac{W_{22}^a}{W_{12}^a} \right) W_{12}^a \\ &= \left(W_{21}^b - W_{22}^b \frac{W_{11}^b}{W_{12}^b} \right) W_{12}^a \\ &= (W_{21}^b W_{12}^b - W_{22}^b W_{11}^b) \frac{W_{12}^a}{W_{12}^b} \\ \lambda &= -\frac{W_{12}^a}{W_{12}^b} = -\frac{w_a(a)}{w_b(b)}. \end{aligned} \quad (28)$$

In the last step we have used the form of W as in eq. 3.

What this tells us is that to make the eigenvalue as small as possible, we must make the $w_a(x)$ solution as small as possible at the right edge of the a part-cell, and conversely, $w_b(x)$ as large as possible at the right edge of the b part-cell.

The above is true for *any* division of the cell into two parts. In the system studied by Capasso et al., the logical division is into the two layers of GaInAs and AlInAs. In that situation, the off-diagonal elements have the form $W_{1,2}^c = -\sin k_c c / \nu_c$ where $\nu_c = k_c / m_c^*$ ($c = a, b$) is the velocity. If the Bragg reflection condition holds, then $\sin k_c c = \pm 1$ and $\lambda = -\nu_b / \nu_a$ is just the ratio of velocities in the two parts of the cell. (This is analogous to the problem of waves on a string, with one part thin and the

other thick. At the join, the displacement $y(x)$ is continuous, and the ratio of the slopes $y'(L)/y'(R)$ is the ratio of the velocities squared.) One sees that in the a -cell, the solution $w_a(x)$ rises to the value $w_a(a) = 1/\nu_a$, while starting from d and moving backwards through the barrier region, the corresponding solution falls to the value $w_b(-b) = -w_b(b) = -1/\nu_b$. Normalizing the b solution to ensure continuity at $x = a$ requires the factor λ .

The result eq. 28 is quite amazing because in the general situation where the potential and effective mass vary arbitrarily, the dividing line can be placed wherever you wish. To make the eigenvalue small, one must make the “odd-parity” solution $w(x)$ as large as possible everywhere in the second part-cell and as small as possible in the first. As observed by Weber, the first aspect can be achieved by choosing an energy just above the barrier (small k_b). To meet the Bragg condition, this forces a large b , and the linear variation of $w_b(x)$ over the barrier leads to a large wave function at $x = b$. That is why lowering the energy of the CBS in general improves confinement.

However, our aim is to improve confinement while *keeping the energy of the CBS fixed*. To do so, we are guided by Shockley’s explanation for the existence of surface states, as discussed in⁹. We split the a part-cell into two sections, a_1 , a_2 , making the left side more attractive, and the right side less so ($V_{w1} < V_w < V_{w2}$). Then the greater curvature of w_a near the origin, balanced by less curvature to the right, will lead to a smaller value of $w_a(a)$, even if the average attraction is the same. We leave the b -cell fixed, but a similar strategy with less repulsion on the right side, can obviously be employed there.

To illustrate this, we have selected a set of heterostructures based on quaternary alloys $Ga_x In_{1-x} As_y P_{1-y}$, lattice-matched to InP ($x = 0.468y$). We took information from Figs. 1.17 (for band gaps) and 1.20 (for effective masses) of Swaminathan and Macrander¹⁴. For the band offsets, S. Adachi¹⁵ gives

$$\begin{aligned} \Delta E_c &= 268y + 3y^2 \\ \Delta E_v &= 502y - 152y^2 \end{aligned} \quad (29)$$

The band alignments are also discussed on p. 87 of Davies¹⁶. Putting together this information, we arrived at the following set of parameters:

$$\begin{aligned} y = 1.0 & \quad m_0^* = 0.043 \quad \bar{E}_g = 0.880 \text{ eV} \\ y = 0.5 & \quad m_0^* = 0.061 \quad \bar{E}_g = 1.080 \text{ eV} \\ y = 0.0 & \quad m_0^* = 0.081 \quad \bar{E}_g = 1.360 \text{ eV} \end{aligned} \quad (30)$$

where \bar{E}_g are effective band gaps in the sense of Nelson et al.¹¹.

In this way we can have conduction band potential steps of 125 meV (from $Ga_{.47}In_{.53}As$ to $Ga_{.23}In_{.77}As_{.5}P_{.5}$ or 250 meV to InP ($y = 0$). These are a quarter (denoted Q) or a half (denoted H) step up to the 500 meV barrier of $Al_{.48}In_{.52}As$.

As our baseline, (denoted (Q, Q) below), we take the a -well to consist entirely of Q ($y = 0.5$) material, so the potential floor at 125 meV is 375 meV below the barrier. The barrier width was fixed at 44.3\AA which satisfies the Bragg condition. For a width $a = 15.82\text{\AA}$, the CBS is at 63 meV above the top of the barrier, as in the original experiment. The eigenvalue $\lambda = -0.4026$, which is not as favorable as in the original work because the well is not so deep. (Capasso et al. selected the materials to have the greatest possible well-barrier potential difference.) The potential properties are summarized in Table IV, top line.

Next we divide the a -well into two parts, one of $GaInAs$ ($y = 1$) and the other of InP . We adjusted the widths a_1 and a_2 to keep E_{CBS} fixed. In the second line of Table IV, denoted $(0, H)_1$, the two part wells are of equal width 9.353\AA , and the eigenvalue is $\lambda = -0.396$. In the third line, denoted $(0, H)_2$, the deeper well has width $a_1 = 10.50\text{\AA}$, and the shallower part $a_2 = 7.911\text{\AA}$, giving $\lambda = -0.374$. This may seem a small gain, but we shall see that the improvement is significant.

We then computed the CBS properties for a finite array based on the above materials, with results shown in Tables V, VI and Fig. 13. The transition strength is significantly narrower and more strongly peaked for the split-well examples. The strength to the bound states in the split-well cases was only 25-30% of that of the (Q, Q) reference case, and the strength to the continuum states was much larger. The results are summarized in Table V, where the number of cells means the number of Bragg reflectors placed on each side of the central defect.

The differences in the total strength are reflected in the portion concentrated in the CBS peak. The decay constant strongly influences both the sharpness of, and the area under, the peak. The cases with a lower (in magnitude) decay constant have narrower, and larger (in terms of area) peaks in the transition strength curve as seen in Table VI.

Overall, the decay constant has a significant effect on both the total strength, and its continuum and bound state contributions individually. A lower value of the decay constant (in magnitude) results in better confinement of the CBS as is evidenced by the width of the peak in the transition strength curve. We conclude that the split-well strategy can produce much better confinement of the CBS. It should be feasible to confirm this method of improving the confinement of CBS, experimentally.

VII. CONCLUSION

We have shown that Continuum Bound States are closely related to surface states, because both arise as a result of perturbing an infinite periodic system. The results of Weber³ concerning the experiment of Capasso et al. were verified. However, while we confirm that a CBS can exist even when the Bragg conditions are not well satisfied, we note that for this type of potential, one can

prove analytically that optimal confinement is achieved by the Bragg conditions. In addition, by enclosing a finite array in a box, we have traced the evolution of the Bloch states in the allowed bands as the number of Bragg layers is increased.

We have derived a sum rule, within the conduction band only model, that explains the integrated transition strength from the ground state to the continuum in the region where the CBS exists. About 70% of the sum rule strength is concentrated in this region. Finally, we have identified the factors that allow one to improve the confinement of a continuum bound state, and proposed a way of testing this.

ACKNOWLEDGMENTS

We are grateful to NSERC-Canada for research grant SAPIN-3198 (DWLS) and Summer Research Awards (PJ, JS), and to DGES-Spain for continued support through grant PB97-0915 (JM). This work was carried out as part of CERION, an Esprit project EP-27119 funded by the EU and NSERC.

APPENDIX A: SUM RULE FOR INTRA-SUBBAND TRANSITIONS

Sirtori et al.¹³ discussed the sum rule for excitations to the CBS within a two-band Kane model. Here we limit our discussion to what can be done within a conduction-band only model, eq. 1. The difficulty which arises in this context is that having an energy-dependent effective mass means that the Hamiltonian does not have a complete orthonormal set of excited states, so the sum rule can only be approximate.

We take the operator to be

$$-i\hbar S = \left(p\frac{1}{m_E} + \frac{1}{m_0}p\right) \quad (\text{A1})$$

(cf. eq. 16.) Then the sum rule is

$$\begin{aligned} \hbar^2 M_2 &= \hbar^2 \langle 0|S^\dagger S|0\rangle \\ &= \langle 0|(p\frac{1}{m_0} + \frac{1}{m_E}p)(p\frac{1}{m_E} + \frac{1}{m_0}p)|0\rangle \\ &= \langle 0|p\frac{1}{m_0}\frac{1}{m_0}p|0\rangle + \langle 0|p\frac{1}{m_0}\frac{1}{m_E}p|0\rangle - \\ &\quad i\hbar \langle 0|p\frac{1}{m_0}(\frac{1}{m_E})'|0\rangle + \langle 0|p\frac{1}{m_E}\frac{1}{m_0}p|0\rangle + \\ &\quad i\hbar \langle 0|(\frac{1}{m_E})'\frac{1}{m_0}p|0\rangle + \langle 0|p\frac{1}{m_E}\frac{1}{m_E}p|0\rangle + \\ &\quad i\hbar \langle 0|(\frac{1}{m_E})'\frac{1}{m_E}p|0\rangle - i\hbar \langle 0|p\frac{1}{m_E}(\frac{1}{m_E})'|0\rangle \\ &\quad + \hbar^2 \langle 0|(\frac{1}{m_E})'(\frac{1}{m_E})'|0\rangle, \end{aligned} \quad (\text{A2})$$

$$M_2 = \int |\psi'_0|^2 \left(\frac{1}{m_0} + \frac{1}{m_E}\right)^2 dx + \langle 0 | \left(\frac{1}{m_E}\right)' \left(\frac{1}{m_E}\right)' | 0 \rangle + 2 \int \psi_0 \psi'_0 \left(\frac{1}{m_0} + \frac{1}{m_E}\right) \left(\frac{1}{m_E}\right)' dx \quad (\text{A3})$$

To obtain this expression we moved the p -operators until they act on the ground state wave function directly. In the case of a constant effective mass, $m_0 = m_E = 1$, only the first integral survives. In this case the sum rule must be exact, and we found close agreement between the sum rule expression, and direct integration:

$$M_2 = \int \langle \psi_0 | S^\dagger | \psi_E \rangle \frac{dk}{dE} \langle \psi_E | S | \psi_0 \rangle dE$$

where

$$\frac{dk}{dE} = \frac{1}{2k} \frac{2m}{\hbar^2} m_{0b} \left(1 + \frac{2(E - V_b)}{E_b}\right) \quad (\text{A4})$$

which includes non-parabolicity. The wave number k is defined by the energy above the barrier. At high energy the density of states tends to a constant, rather than going to zero, as it would for constant mass. The case without energy-dependence can be recovered if $E_b \rightarrow \infty$. The density of states factor was tested by doing the integrals either over energy or over wave number k .

When we introduce x -dependence to the effective mass, the terms involving the derivative of $(1/m_E^*)$ contribute. Because in this model the mass is piecewise constant, the derivative is a Dirac delta function times the discontinuity in $(1/m_E^*)$. The integral in the last line of eq. A3 is then a sum of values evaluated at the layer edges.

When we introduce energy-dependence as well, both here, and in the first integral, factors such as ψ'_0/m_E are discontinuous, because the mass m_E is taken at one energy and the ground state wave function at another. To resolve this ambiguity we took the average of the two values on either side of the discontinuity. For these materials, the well and barrier masses are similar, so it is not a large uncertainty. This is the stage at which the sum rule can only be approximate. Moreover, we need a prescription for the energy E at which we evaluate m_E . Thinking in terms of the doorway state approximation, initially we took the CBS energy.

The second term in eq. A3 involves the square of a Dirac delta function, and is undefined. We simply omit this contribution.

- ⁵ J. Radovanović, D. Indjin, V. Milanović and Z. Ikonić, Solid State Comm. **110** (1999) 339-343.
- ⁶ Xue-Hua Wang, Ben-Yuan Gu, Guo-Zhen Yang and Jian Wang, Phys. Rev. **B58** (1998) 4629-35.
- ⁷ Wm. Shockley, Phys. Rev. **59** (1939) 319-323.
- ⁸ D.W.L. Sprung, Hua Wu and J. Martorell, Am. J. Phys. **61** (1993) 1118-24.
- ⁹ D. W. L. Sprung, J.D. Sigetich, Hua Wu and J. Martorell, Am. J. Phys. **68** (2000) 715-22.
- ¹¹ D.F. Nelson, R.C. Miller and D.A. Kleinman, Phys. Rev. B **35** (1987) 7770-3.
- ¹² T.M. Kalotas and A.R.Lee, Euro. J. Phys. **16** (1995) 119-23.
- ¹³ C. Sirtori, F. Capasso, J. Faist, and S. Scandolo, Phys. Rev. B **50** (1994) 8663-74.
- ¹⁴ V. Swaminathan and A.T. Macrander, "Materials aspects of GaAs and InP based structures", Prentice Hall, New Jersey, (1991) pp. 1-42
- ¹⁵ S. Adachi, "Physical Properties of III-V Semiconductor Compounds", Wiley Interscience, New York (1992) pp. 96-9.
- ¹⁶ John H. Davies, "Physics of Low-dimensional Semiconductors", Cambridge U.P. (1998).

TABLE I. CBS properties varying widths a and b separately, for a central well.

Central Well					
a	b (Å)	E (meV)	λ_-	$k_w a$	$k_b b$
16	16	686	-0.565	1.876	1.011
16	20	645	-0.499	1.797	1.105
16	30	589	-0.389	1.684	1.275
16	39	563	-0.327	1.632	1.383
16	50	545	-0.277	1.595	1.483
16	60	534	-0.244	1.574	1.557
16	75	525	-0.210	1.555	1.647
16	100	516	-0.173	1.537	1.767
16	125	512	-0.150	1.528	1.862
16	150	509	-0.135	1.522	1.942
16	200	505	-0.115	1.516	2.072
10	39	666	-0.601	1.149	2.320
11	39	651	-0.545	1.243	2.202
12	39	635	-0.493	1.332	2.071
13	39	618	-0.444	1.416	1.926
14	39	600	-0.400	1.494	1.765
15	39	581	-0.361	1.566	1.585
17	39	544	-0.298	1.693	1.148
18	39	525	-0.273	1.750	0.860
19	39	506	-0.251	1.801	0.426

¹ F. Capasso, C. Sirtori, J. Faist, D.L. Sivco, S- N.G. Chu and A.Y. Cho, Nature **358** (1992) 565-7; C. Sirtori *et al.* App. Phys. Lett. **61** (1992) 898-900.

² G. Lenz and J Salzman, App. Phys. Lett. **56** (1990) 871-4.

³ T.A. Weber, Solid State Comm. **90** (1994) 713-6.

⁴ B. Sung, H.C. Chui, E.L. Martinet and J.S. Harris Jr., Appl. Phys. Lett. **68** (1996) 2720-22.

TABLE II. CBS properties varying widths a and b separately for a central barrier.

Central Barrier					
a	b (Å)	E (meV)	λ_-	$k_w a$	$k_b b$
16	16	778	-0.626	2.058	1.273
16	20	715	-0.555	1.934	1.372
16	30	620	-0.430	1.747	1.496
16	39	577	-0.354	1.661	1.539
16	50	549	-0.289	1.605	1.561
16	60	535	-0.246	1.575	1.570
16	75	523	-0.200	1.550	1.575
16	100	513	-0.153	1.530	1.577
16	125	508	-0.123	1.521	1.577
16	150	506	-0.103	1.516	1.576
16	200	503	-0.077	1.511	1.575
10	39	602	-0.443	1.070	1.785
11	39	597	-0.416	1.169	1.734
12	39	592	-0.396	1.268	1.689
13	39	588	-0.379	1.367	1.648
14	39	584	-0.368	1.465	1.609
15	39	581	-0.359	1.563	1.573
17	39	574	-0.351	1.757	1.505
18	39	571	-0.352	1.854	1.472
19	39	568	-0.356	1.950	1.439

TABLE III. CBS properties for fixed energy 560 eV.

Energy fixed at 560 meV					
a	b (Å)	Energy	λ_-	$k_w a$	$k_b b$
10	77.29	560.00	-0.591	1.016	2.671
13	65.14	560.00	-0.393	1.321	2.251
14	58.25	559.99	-0.345	1.423	2.013
15	49.70	559.98	-0.318	1.524	1.717
15.4	45.98	560.00	-0.315	1.565	1.589
15.45	45.51	560.01	-0.315	1.570	1.573
15.455	45.465	560.01	-0.315	1.5706	1.5713
15.457	45.449	560.00	-0.315	1.57084	1.57065
15.46	45.42	560.00	-0.315	1.5712	1.5597
15.5	45.05	560.00	-0.315	1.575	1.557
16	40.45	559.96	-0.319	1.626	1.397
17	31.99	560.01	-0.348	1.727	1.106
18	25.25	560.01	-0.398	1.829	0.873
19	20.16	560.02	-0.460	1.931	0.697
20	16.33	560.03	-0.527	2.033	0.564

TABLE IV. Optimized three-layer potentials indicating the changes in the widths a_1 , a_2 , $w(a)$, $\nu_a = k_a/m_a^*$, and eigenvalue λ . In all cases $b = 44.2851450\text{Å}$, $w_b(b) = 2.1450935$, and $E_{CBS} = 563.0$ meV.

case	a_1	a_2	$w(a)$	ν_a	λ
(Q, Q)	7.9109	7.9109	0.8636	1.1579	-0.4026
$(0, H)_1$	9.3535	9.3535	0.8495	0.9092	-0.3960
$(0, H)_2$	10.4995	7.9109	0.8031	0.9092	-0.3744

TABLE V. Evolution of the transition strength (\AA^{-2}) with increasing number of Bragg reflectors.

# Cells	Bound			Continuum			Total Strength		
	(Q,Q)	(0, H) ₁	(0, H) ₂	(Q,Q)	(0, H) ₁	(0, H) ₂	(Q,Q)	(0, H) ₁	(0, H) ₂
0	0	0	0	0.912	1.279	1.324	0.912	1.279	1.324
1	0.108	0.0267	0.0319	0.762	1.188	1.234	0.870	1.215	1.266
2	0.117	0.0281	0.0334	0.759	1.188	1.233	0.876	1.216	1.267
3	0.118	0.0282	0.0335	0.754	1.183	1.229	0.872	1.211	1.263
4	0.118	0.0282	0.0335	0.746	1.176	1.224	0.864	1.204	1.257
5	0.118	0.0282	0.0335	0.745	1.174	1.225	0.863	1.202	1.258

TABLE VI. Total strength under the CBS peak: dependence on number of Bragg reflectors.

Cells	Peak Height $\text{eV}^{-1}\text{\AA}^{-2}$			Width Γ (eV)			Peak/Total Strength (%)		
	(Q,Q)	(0, H) ₁	(0, H) ₂	(Q,Q)	(0, H) ₁	(0, H) ₂	(Q,Q)	(0, H) ₁	(0, H) ₂
1	27.5	38.2	45.6	$1.73 * 10^{-2}$	$1.49 * 10^{-2}$	$1.33 * 10^{-2}$	85.8	73.7	75.5
2	165.	247.	328.	$2.42 * 10^{-3}$	$2.07 * 10^{-3}$	$1.68 * 10^{-3}$	71.6	66.1	68.4
3	1026.	1609.	2383.	$3.81 * 10^{-4}$	$3.16 * 10^{-4}$	$2.33 * 10^{-4}$	70.5	66.0	69.1
4	6300	10240	16970.	$6.18 * 10^{-5}$	$4.92 * 10^{-5}$	$3.24 * 10^{-5}$	70.8	65.7	68.7
5	38950	65450	121300	$1.00 * 10^{-5}$	$7.76 * 10^{-6}$	$4.54 * 10^{-6}$	71.0	66.4	68.8

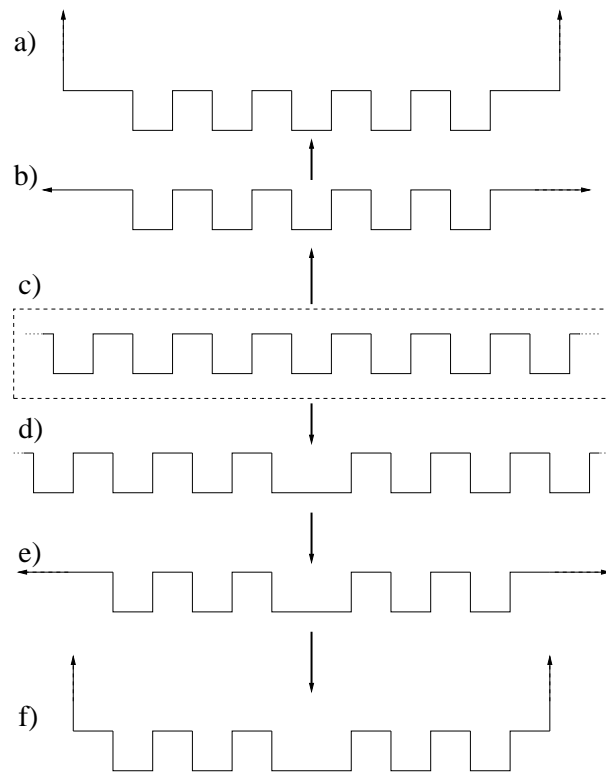


FIG. 1. Schematic drawing of an infinite array (line c), truncated to a finite array (b) and enclosed in walls (a); or with a defect (d), also truncated (e) and enclosed (f).

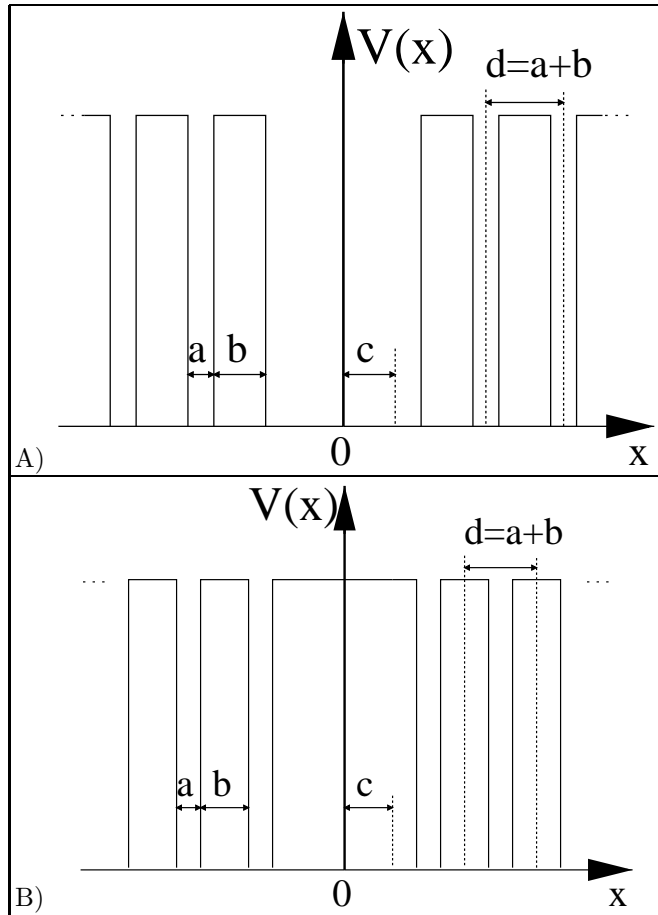


FIG. 2. A unit cell of the infinite lattice for A) a well as the central defect, and B) a barrier as the central defect.

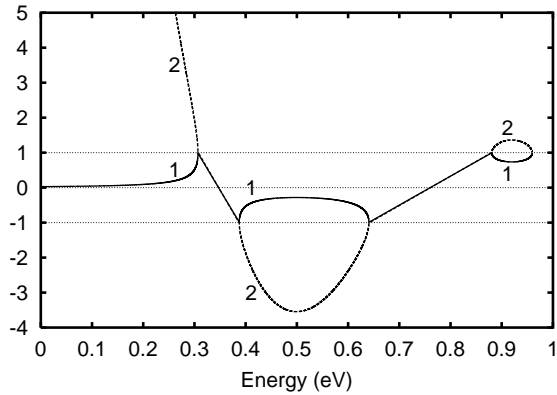


FIG. 3. Eigenvalues vs. energy for a central well, $c = 8\text{\AA}$, showing the smaller magnitude eigenvalue λ_- (line 1) and the larger λ_+ (line 2). The straight lines across the allowed zones (where the λ_{\pm} are complex) connect related solutions.

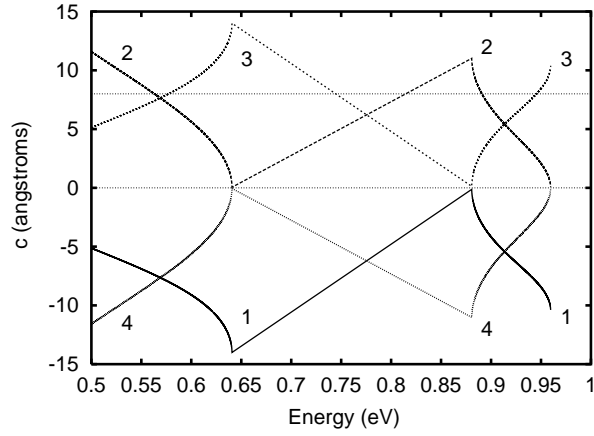


FIG. 4. Central well width c versus energy showing the even CBS (line 1), the odd CBS (line 2), the even ABS (line 3), and the odd ABS (line 4). See also figure 6. The straight lines across the allowed zones connect related solutions.

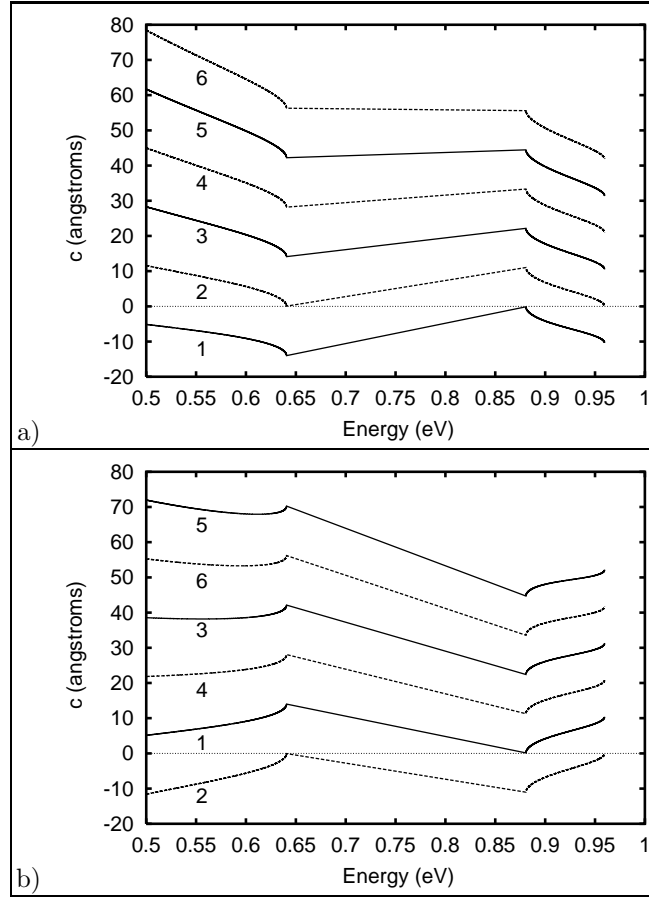


FIG. 5. Central well width c versus energy showing a) the CBS and b) the ABS. Odd numbered lines are for even states, and vice versa. The straight lines across the allowed zone connect related solutions.

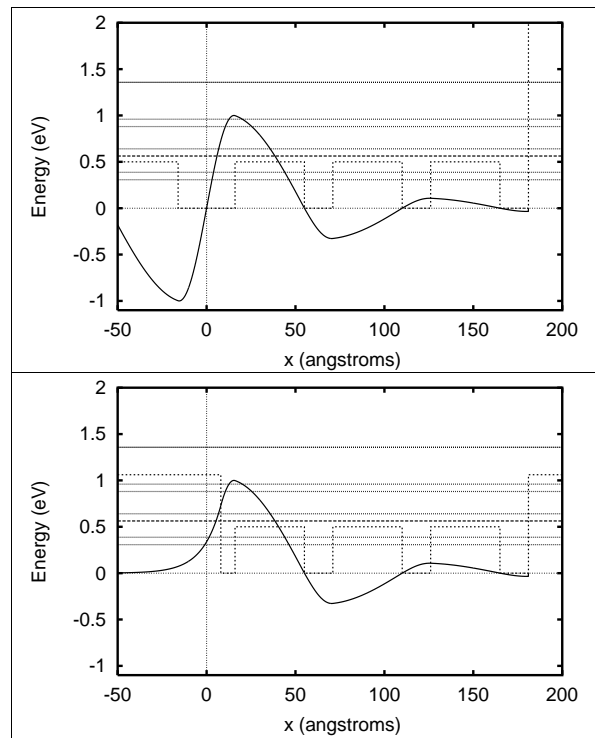


FIG. 6. Wave functions of a CBS (a) and a surface state (b) compared.

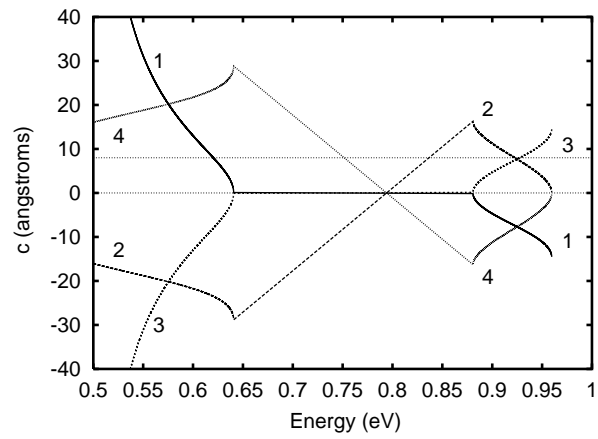


FIG. 7. Same as Fig. 4 but for a central barrier. (The straight lines across the allowed zone connect related solutions.)

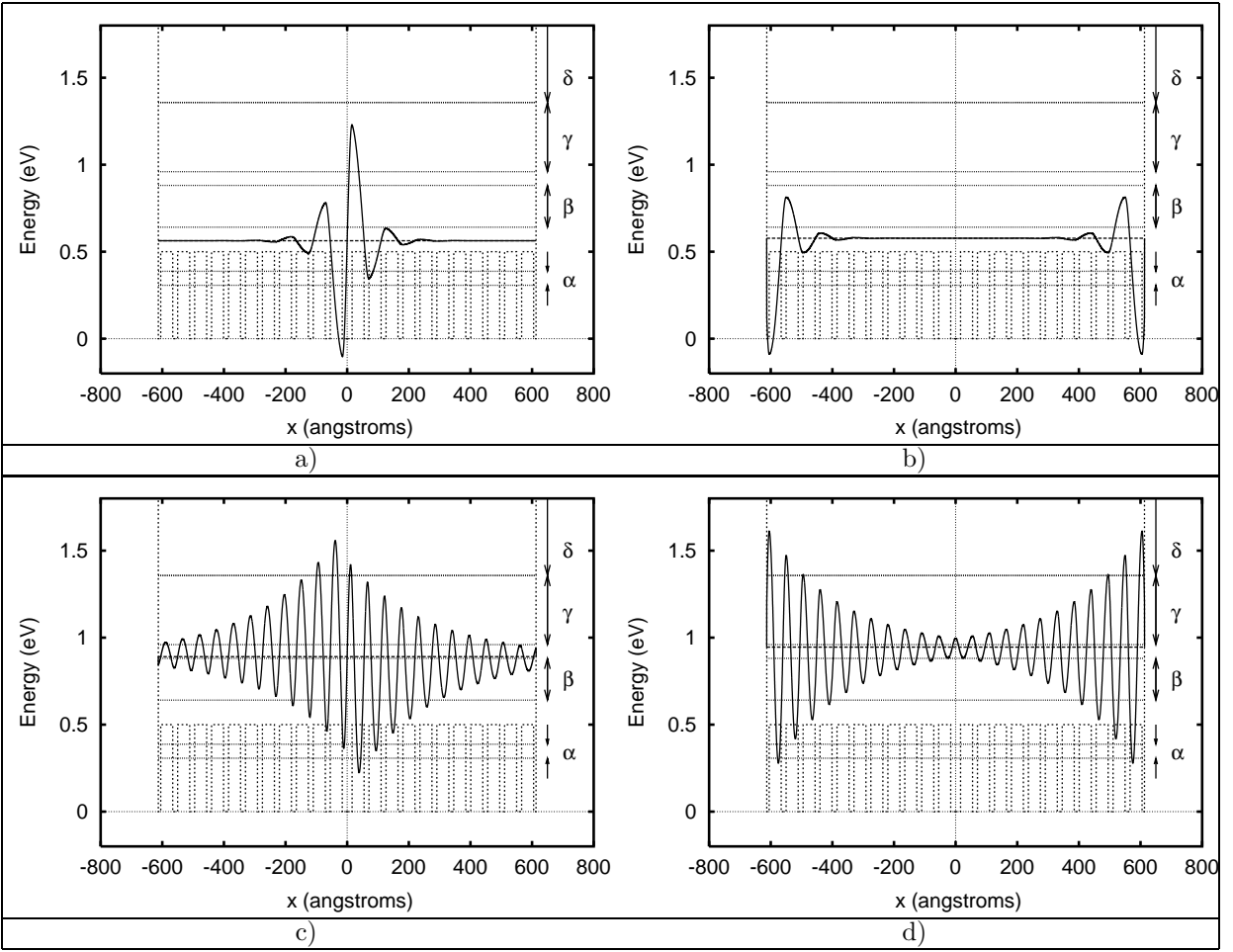


FIG. 8. States in a box, for $c=8\text{\AA}$, also showing a) the CBS at 563 meV, b) the ABS at 577 meV, c) the CBS at 891 meV and d) the ABS at 946 meV. At right, α labels the first allowed band from $307\rightarrow 387$ meV, β the second allowed band from $641\rightarrow 881$ meV, γ the third allowed band from $960\rightarrow 1357$ meV, and δ the fourth allowed band from 1357 meV. Dotted lines show the potential cells, in eV; wave functions are dimensionless and are drawn with base line at the energy eigenvalue.

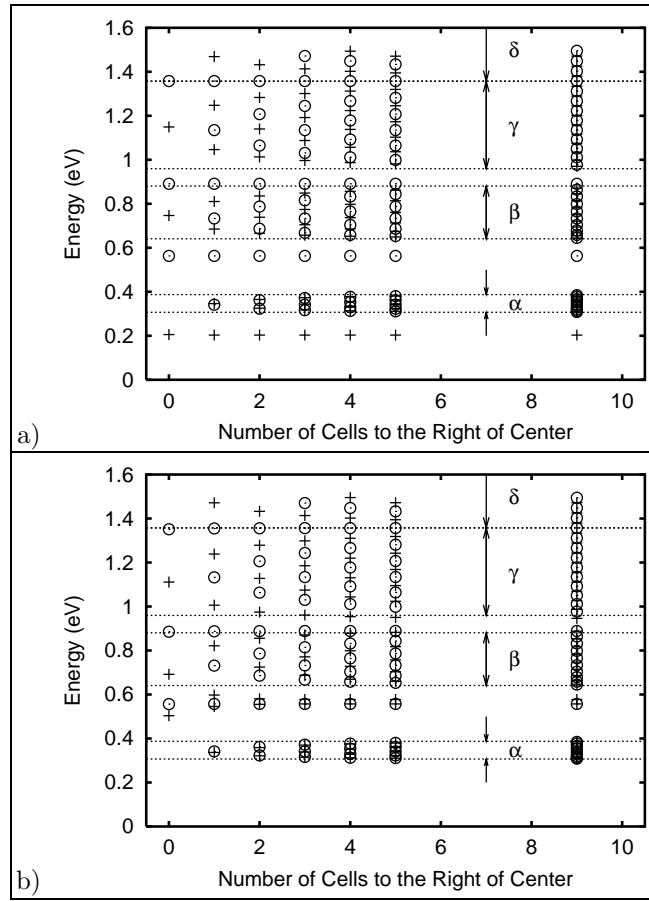


FIG. 9. Even (+) and odd (O) state energies (in a box) versus number N of cells to the right of the central defect. Panel a) is for a central well, and b) a central barrier. Bands labelled as in Fig. 8.

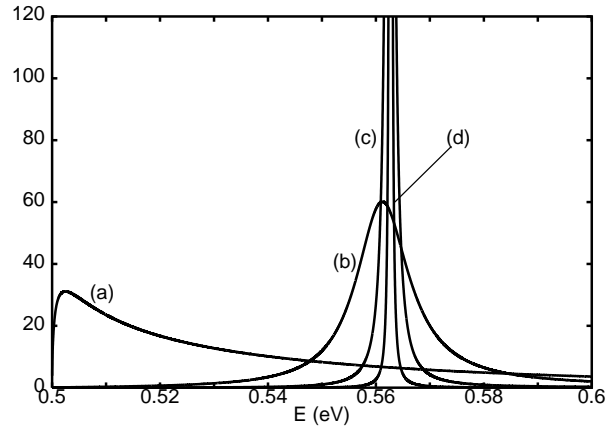


FIG. 10. The transition strength times density of states (units $\text{eV}^{-1} \text{Å}^{-2}$) for a) a central well of width 32Å , and a central well surrounded by b) one cell, c) two cells, and d) three cells on each side.

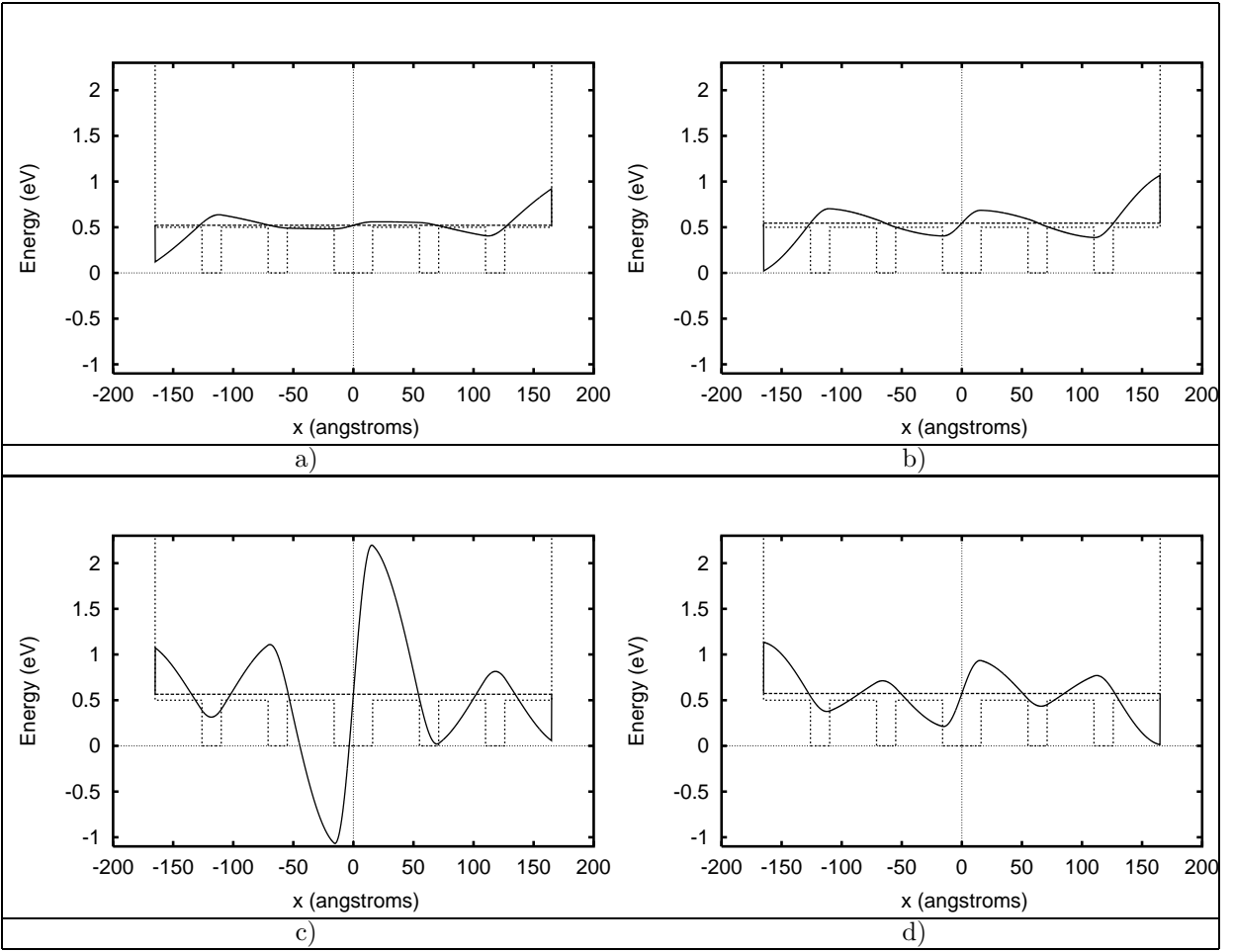


FIG. 11. Four representative continuum wave functions, for $c=8\text{\AA}$, at energies $E = 521\text{ meV}$ (a); 545 meV (b); 565 meV (c); and 573 meV (d). Dotted lines show the potential cells, in eV; wave functions are dimensionless and are drawn with base line at the corresponding energy.

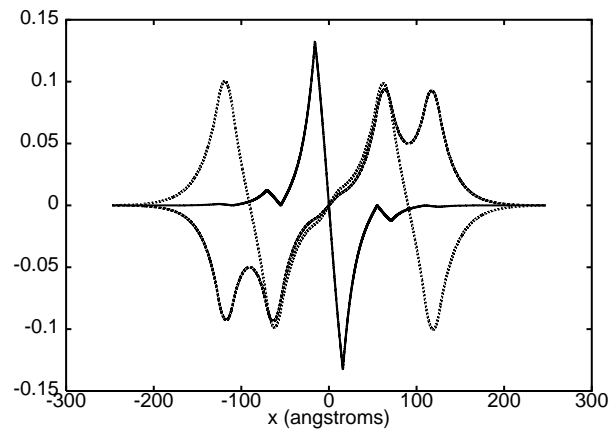


FIG. 12. The derivative of the ground state wave function (over m^*) a) and the first and second odd-parity excited wave functions, b) and c), for a 5 well potential (two identical cells on each side of a central well), enclosed in a box, illustrating the similar overlap near the origin.

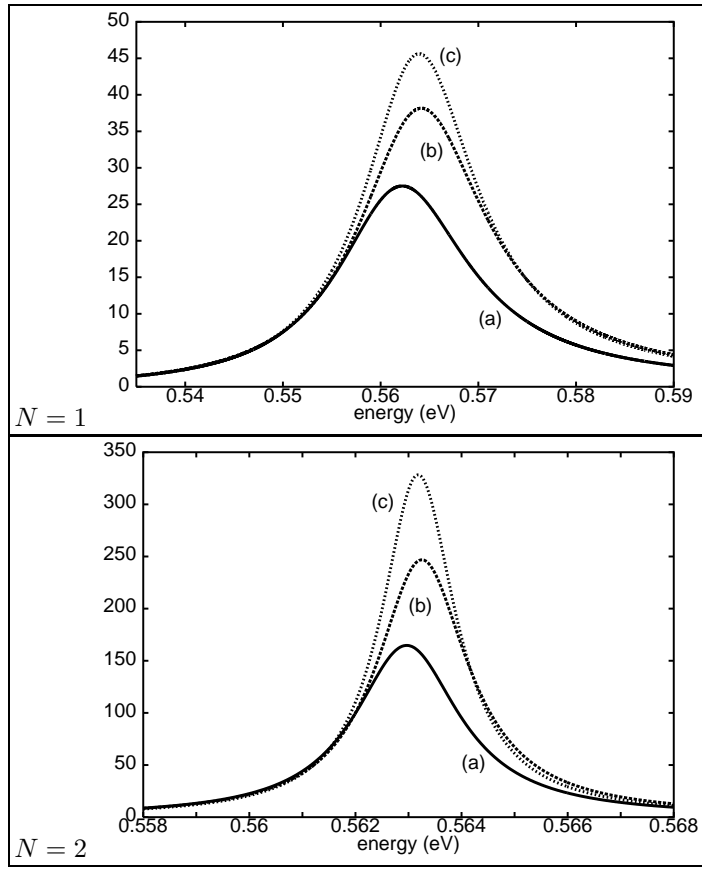


FIG. 13. Transition strength to continuum (units $\text{eV}^{-1} \text{\AA}^{-2}$) for (a): case (Q, Q) , (b): $(0, H)_1$, and (c): $(0, H)_2$, showing the evolution of the CBS peak. Note change of scale between the upper panel for $N = 1$ reflector and the lower panel for two.